To appear in:
International Journal of Nano Dimension (Int. J. Nano Dimens.)

Online ISSN: 2228-5059 Print ISSN: 2008-8868

Dates:
Received: 20 August 2025
Revised: 15 September 2025
Accepted: 18 September 2025

DOI: https://doi.org/10.57647/ijnd-2026-1702-03

Research Paper

Influence of tannic acid pH on the crystallographic structure and electrical properties of ZnO nanostructured thin films

Aqilah Kamaruzaman[1, 2], Nurul Akmal Che Lah[1, *]

[1]*Faculty of Manufacturing and Mechatronics Engineering Technology, Universiti Malaysia Pahang Al-Sultan Abdullah, 26600, Pekan, Pahang, Malaysia*
[2]*Faculty of Engineering, City University Malaysia, 3500, Jalan Teknokrat 3, Cyber 4, 63000 Cyberjaya, Selangor, Malaysia*

[*]Corresponding e-mail: akmalcl@umpsa.edu.my

Abstract

This study presents a comprehensive investigation into the structural, chemical, and electronic properties of zinc oxide (ZnO) and tannic acid-functionalized ZnO (ZnO–TA) nanostructures, synthesized via a green hydrothermal route under controlled pH conditions. FESEM revealed that pristine ZnO crystallized into well-defined nanorods, whereas incorporation of TA at acidic pH values induced a morphological transition towards interconnected networks, concomitant with elevated carbon incorporation. FTIR confirmed the presence of Zn–O vibrational modes alongside characteristic peaks corresponding to carbonyl, ester, and hydroxyl functionalities, evidencing successful surface modification by TA. The four-point probe I–V measurements demonstrated linear ohmic behaviour and a significant enhancement in lateral conductivity, reaching up to 10^{-8} S·cm^{-1}, surpassing previously reported benchmarks for similar systems. Hall effect measurements consistently indicated n-type conductivity across all samples. Notably, carrier mobility peaked at pH 5, attributed to effective passivation of surface trap states by TA's functional groups. In contrast, excessive TA loading at pH 3 resulted in increased carrier concentrations but diminished mobility, likely due to nanoparticle aggregation and enhanced grain boundary scattering. These findings demonstrate the pivotal influence of pH and TA concentration in tailoring the morphology, surface chemistry and charge transport characteristics of ZnO nanostructures.

Keywords: Green Hydrothermal Synthesis; Nanostructures; PET Thin Film; Tannic Acid; ZnO.

1. Introduction

Zinc oxide (ZnO) nanostructures constitute a highly adaptable class of semiconducting materials, characterized by a wide direct bandgap (~3.37 eV), high exciton binding energy (~60 meV), commendable electron mobility and intrinsic optical transparency. These attributes, coupled with their natural *n*-type conductivity at ambient conditions [1, 2], position ZnO as a compelling candidate for integration into a broad spectrum of advanced technologies, including gas sensors, light-emitting diodes, transparent electronics, and next-generation photovoltaic systems [3]. The functional efficacy of ZnO nanostructures is intimately governed by their morphology, crystallinity and surface chemistry, in which parameters that are, in turn, strongly influenced by synthesis conditions such as pH, precursor concentration, and reaction temperature. Among the various fabrication techniques available, ranging from sol–gel and wet-chemical methods to hydrothermal and green synthesis, the hydrothermal approach has emerged as particularly advantageous. It offers precise control over structural features, scalability and environmental compatibility [4, 5], making it a preferred route for producing well-defined ZnO nanostructures [6,7]. Recent studies have demonstrated that hydrothermal synthesis not only enables morphological control but also enhances electrochemical and dielectric properties, particularly when combined with organic modifiers or dopants. For instance, ZnO composites have shown improved dielectric behaviour and charge transport characteristics when modified with biocompatible agents or integrated into hybrid systems [8]. Moreover, the incorporation of organic molecules has been shown to influence the vibrational and bonding characteristics of ZnO, as evidenced by FTIR and Raman analyses, which reveal shifts in functional group interactions and lattice dynamics [9].

Green synthesis strategies offer significant advantages in terms of cost-efficiency, reproducibility and procedural simplicity, making them highly suitable for the sustainable synthesis of nanomaterials [10]. Recent efforts have increasingly focused on synthesis routes that utilize naturally derived biomolecules to enhance the functional performance of ZnO nanostructures while minimizing the environmental impact of conventional chemical processes. Among these, hydrothermal synthesis using plant-based compounds has gained attention for its ability to produce ZnO nanostructures without relying on harsh chemical or physical reducing agents [10]. In this context, tannic acid (TA), a naturally occurring polyphenolic compound sourced from plant materials and trisodium citrate are employed as eco-friendly reducing and stabilizing agents. Their use, combined with water as the reaction medium under controlled temperature and pressure, aligns with the principles of green chemistry. This approach not only reduces ecological footprint and production costs but also supports the classification of the process as a green hydrothermal method. Structurally defined as *penta-m*-digalloyl glucose, TA represents one of the simplest hydrolysable tannins and is widely recognized for its antioxidant, anti-mutagenic, and antimicrobial properties [11–14]. These characteristics make TA a promising candidate for green nanomaterial synthesis and surface functionalization. Rich in

hydroxyl and carboxyl functional groups, TA serves as an effective capping and stabilizing agent, capable of forming strong electrostatic interactions with nanostructure surfaces. These functional moieties facilitate coordination with metal ions and active surface sites, further influencing the nucleation and growth kinetics of ZnO nanostructures. Furthermore, the incorporation of organic functional layers via TA may enhance biocompatibility and impart tunable surface properties, offering distinct advantages for applications in biomedical and optoelectronic devices.

While green synthesis offers considerable advantages, the incorporation of TA and variations in synthesis pH exert a pronounced influence on the structural and electronic properties of ZnO nanostructures. Acidic conditions have been shown to enhance ZnO performance, primarily by promoting the nucleation phase, which facilitates the formation of more uniform, densely packed nanostructures with superior functional attributes [15, 16]. Additionally, studies have shown that pH modulation during synthesis can significantly affect the defect density, surface charge distribution, and particle connectivity, which in turn influence the electrical conductivity and sensing performance of ZnO-based materials [17]. In particular, ZnO composites functionalised under acidic conditions have demonstrated enhanced humidity sensing and electrochemical response, attributed to improved surface area and active site availability [18]. However, modifications in surface chemistry, particle agglomeration, and defect distribution which arising from TA incorporation may either augment or impair the performance of ZnO, depending on the concentration and synthesis parameters employed. A nuanced understanding of the interplay between morphology, chemical bonding and electrochemical and electronic behaviour is therefore essential for the rational design and optimization of ZnO-based nanomaterials [17-19]. Such insight is critical to unlocking their full potential across a wide range of applications, including sensing technologies, catalysis, and biomedical engineering [3].

Herein, this study investigates the impact of TA concentration and pH variation on the structural and electronic properties of ZnO nanostructures synthesized via a green hydrothermal method. Morphological evolution was characterized through surface topology and particle distribution analyses, while chemical bonding and functional group identification provided insight into surface modifications induced by TA. Electrical behaviour was assessed through conductivity profiling and carrier transport measurements, enabling a comprehensive evaluation of the structure–property relationships in both pristine ZnO and ZnO–TA systems. By elucidating the correlations between morphology, surface chemistry, and electronic performance, this work establishes a foundational understanding of the synergistic effects arising from TA functionalization and pH modulation during synthesis. Through systematic analysis, the study contributes to bridging the gap between environmentally benign synthesis strategies and the optimization of ZnO-based device performance. Previous investigations have demonstrated that surface modification and composite

formation can markedly influence the functional properties of ZnO-based materials, as exemplified by their electrochemical behaviour in nanocomposite aerogels [19] and humidity sensing capabilities in Ag/ZnO nanotetrapod architectures [20]. The findings presented herein advance the fundamental understanding of structure–function relationships in functional nanomaterials and pave the way for sustainable, scalable approaches to next-generation applications in optoelectronics, sensing, and biomedical engineering.

2. Experimental Methods

2.1 Materials

High purity bulk Zn powder (ZnO, 99.9% purity, analytical grade), 5 mmol (0.15 g) of trisodium citrate flakes (Na3C6H5O7, 99.9% purity, analytical grade) and a 0.1 M tannic acid (TA) solution were obtained from R&M Chemicals. Distilled water was employed throughout all experimental procedures without further purification. The deposition of thin films was carried out on clean polyethylene terephthalate (PET) substrates, each measuring 1 cm × 1 cm in surface area, sourced from Sigma-Aldrich (Malaysia).

2.2 Synthesis of Pure ZnO and ZnO-TA Nanostructures

Both pure ZnO and ZnO-TA nanostructures were synthesized via a hydrothermal approach. Specifically, 0.5 g of Zn powder was dispersed in 100 mL of distilled water under continuous magnetic stirring. Subsequently, 5 mmol (0.15 g) of trisodium citrate ($Na_3C_6H_5O_7$) was introduced as a reducing agent, yielding a white suspension. For the control sample (pure ZnO), the pH was maintained at 7 without the addition of TA. For TA-modified ZnO nanostructures, the synthesis protocol remained consistent, with the exception of adding different volumes of 0.1 M TA solution to adjust the pH: 60 mL for pH 5 and 480 mL for pH 3. Each reaction mixture was transferred to a heating platform enclosed within a vacuum chamber and maintained at 90 °C for 1 hour to facilitate the hydrothermal reaction. Upon completion, the resulting suspensions were centrifuged to remove residual impurities and washed repeatedly with distilled water. The purified products were re-dispersed in distilled water and stored for subsequent thin film deposition onto PET substrates for characterisation.

2.3 Film Deposition

A 1 μL of the prepared pure ZnO and ZnO-TA nanostructure solution was uniformly drop-cast onto a PET thin film using a clean Mayer wire-wound rod #3 (12.7 mm diameter, 406.4 mm length, 0.25 mil wire) with a rolling technique, followed by vacuum drying for 24 hours to obtain the flexible ZnO/PET thin film.

2.4 Characterisation

2.4.1 Surface Morphological Measurement

The surface morphology and elemental composition of the ZnO- and ZnO-TA-based thin films were characterized using high-resolution imaging and compositional analysis techniques. Surface topography was examined via field emission scanning electron microscopy (FESEM; Auriga, Zeiss, Germany), operated at an accelerating voltage of 5 kV. Elemental analysis was performed using energy-dispersive X-ray spectroscopy (EDX), integrated within the LSM880-FESEM system (Carl Zeiss AG, Germany), with imaging capabilities ranging from 50,000× to 100,000× magnification.

For sample preparation, 2 to 3 mL of the ZnO and ZnO-TA nanostructure suspension was dispensed onto aluminium foil and dried into powder form on a heating plate. A glass layer was placed between the foil and the heating surface to prevent direct thermal contact and ensure uniform drying. This procedure was consistently applied across all samples. The dried powders were subsequently mounted onto standard pin stubs and introduced into the FESEM chamber for imaging and elemental analysis.

2.4.2 Functional Groups and Bonding Measurement for the Thin Film

The chemical bonding characteristics and functional groups present in the ZnO and ZnO-TA-based thin films were analyzed using Fourier Transform Infrared (FTIR) spectroscopy (PerkinElmer Spectrum 100, USA), equipped with an attenuated total reflection (ATR) accessory. This configuration enabled the acquisition of high-resolution spectra within the mid-infrared range (4000 to 700 cm^{-1}), with each measurement performed at a spectral resolution of 4 cm^{-1} and comprising three individual scans.

For sample preparation, 2 mL of each suspension was uniformly applied onto a clean glass substrate and dried under ambient conditions within a vacuum chamber for 24 hours to ensure complete removal of residual deionised water and to yield a uniform dry film suitable for infrared analysis. A small quantity of the resulting powdered material was subsequently placed onto the ATR crystal to ensure consistent contact. Infrared radiation was transmitted through the crystal and interacted with the sample to generate absorbance spectra. To improve signal fidelity and spectral accuracy, an average of 30 scans was recorded per sample. The resulting spectra were analyzed to identify functional groups associated with the interaction between the ZnO surface and organic modifiers such as TA.

1.4.3 Electrical Properties Measurement for the Thin Film

Current–voltage (*I–V*) characterisation was conducted using a four-point probe configuration (Jandel Universal Probe) in conjunction with a Keithley 2600B Source Measure Unit (SMU). A uniform contact force of 10 g was applied to each probe, spaced 1 mm apart, to ensure consistent and reliable electrical contact with the thin film surface. Measurements were performed across a frequency range of 10 to 50 Hz to accurately determine sheet resistance. The recorded resistance values encompassed both the intrinsic electrical resistance of the films and the contact resistance at the probe–film interface. The lateral conductivity, σ in S.cm^{-1} was calculated using the following equation:

$$\sigma = \frac{1}{\rho} \tag{1}$$

The resistivity of the film, ρ in Ω is calculated based on the:

$$\rho = R_{sh}t \tag{2}$$

where the $R_{sh}$is sheet resistance in Ω.sq^{-1} with t, the thickness and CF is known for the lateral correction factor for the probe given by:

$$R_{sh} = \frac{\pi}{ln}\left(\frac{V}{I}\right) \approx 4.53\left(\frac{V}{I}\right)CF \tag{3}$$

Meanwhile, the Hall effect measurements were carried out using the HMS ECOPIA 3000 system, employing a probe current of 10 mA and a magnetic field strength of 1 Tesla. Analyses were performed on square-shaped thin films (1 × 1 cm) deposited onto flexible PET substrates with a thickness of 0.5 mm. This configuration enabled precise determination of key electronic parameters, including carrier type (*n*-type or *p*-type), carrier concentration and electron mobility. These metrics are critical for evaluating the suitability of the films for optoelectronic and sensing applications, particularly in relation to surface modifications induced by TA and variations in synthesis pH.

3. Results and Discussion

3.1 Surface Morphology Properties of the Solution Samples

As illustrated in **Figure 1**, the surface morphology of both pristine ZnO and ZnO–TA nanostructures, as revealed by FESEM, demonstrates a distinct evolution from nanorod architectures to quasi-spherical aggregates with increasing TA concentration. At neutral pH (pH 7), the unmodified ZnO sample (**Figure**

1a(i)) exhibits sparsely distributed nanorods with faceted, prism-like morphologies, ranging from tens to several hundreds of nanometers in diameter. The corresponding microscale image (**Figure 1a(ii)**) reveals a heterogeneous distribution of well-defined nanorods, which adhere to one another to form a dense, porous network. This configuration contributes to broad surface coverage and enhanced structural stability.

Upon the introduction of TA at moderate concentration (pH 5), the ZnO–TA sample (**Figure 1b(i)**) displays a more compact and interconnected morphology, with nanorod features no longer discernible. The microscale image (**Figure 1b(ii)**) further confirms the formation of distinct porous clusters, separated by larger voids, indicative of nanorod disaggregation and reassembly into a networked structure. Under highly acidic conditions (pH 3), corresponding to a higher TA concentration, the ZnO–TA sample (**Figure 1c(i)**) exhibits extensive particle aggregation and complete loss of nanorod morphology. The nanoscale surface appears amorphous and sponge-like, while the microscale image (**Figure 1c(ii)**) reveals a continuous, irregular porous layer. These observations suggest that increasing acidity progressively disrupts the nanorod architecture, promoting disaggregation and the formation of a fused nanoparticle network.

To further clarify the elemental composition of the as-synthesized ZnO and ZnO-TA nanostructures samples, EDX was employed alongside FESEM imaging. **Figures 2a**, **2b**, and **2c** present the EDX spectra corresponding to ZnO nanostructure samples synthesized at pH 7, pH 5, and pH 3, respectively. A comparative overview of the elemental weight percentages (wt%) of carbon (C), oxygen (O), and zinc (Zn) is illustrated in **Figure 3**. It is noteworthy that the presence of aluminium (Al) in **Figure 3a** arises from the use of Al foil as a substrate during sample preparation. Although the same substrate was employed for all samples, Al was not detected in the pH 7 samples, likely due to the sparse and well-defined distribution of isolated ZnO nanorods, which left portions of the substrate exposed. In contrast, the ZnO–TA samples synthesized at pH 5 and pH 3 exhibited denser and more interconnected morphologies, effectively covering the substrate and thereby masking the Al signal. The pristine ZnO sample synthesized at pH 7 exhibited a dominant Zn content of 72.49%, followed by O at 17.46%, with C either absent or present in negligible quantities, consistent with the expected stoichiometry of pure ZnO. In contrast, C was detected exclusively in the ZnO–TA samples synthesized at pH 5 and pH 3 (**Figures 3b** and **3c**), attributable to the phenolic and carboxylate functional groups of tannic acid. These findings suggest that TA incorporation, modulated by pH, significantly influences both the morphology and elemental composition of the resulting nanostructures.

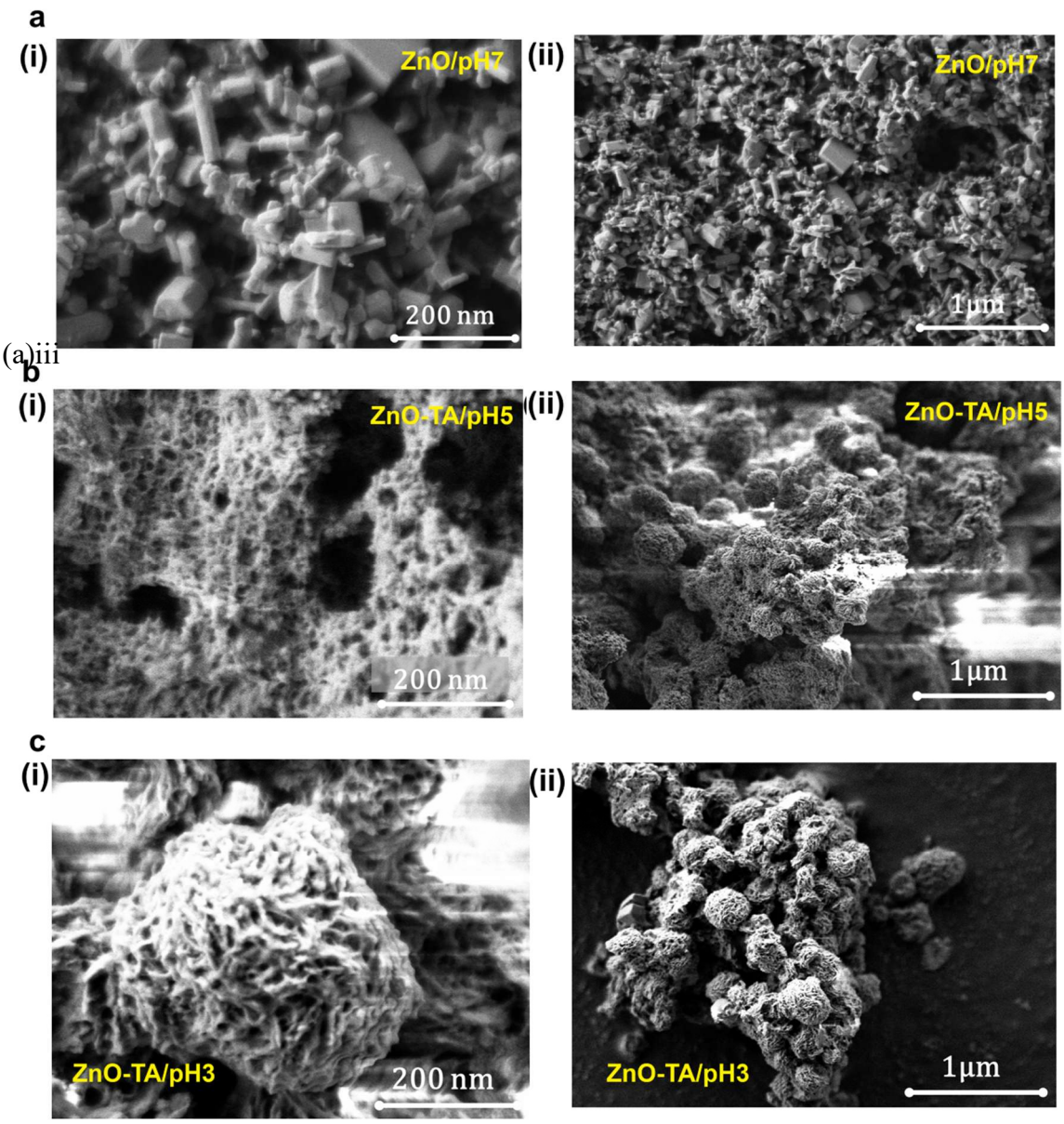

Figure 1: Surface morphology of ZnO-based nanostructures synthesized via the hydrothermal method: (a) ZnO at pH 7, (b) ZnO–TA at pH 5, and (c) ZnO–TA at pH 3. Each sample is shown at (i) nanoscale resolution and (ii) microscale resolution.

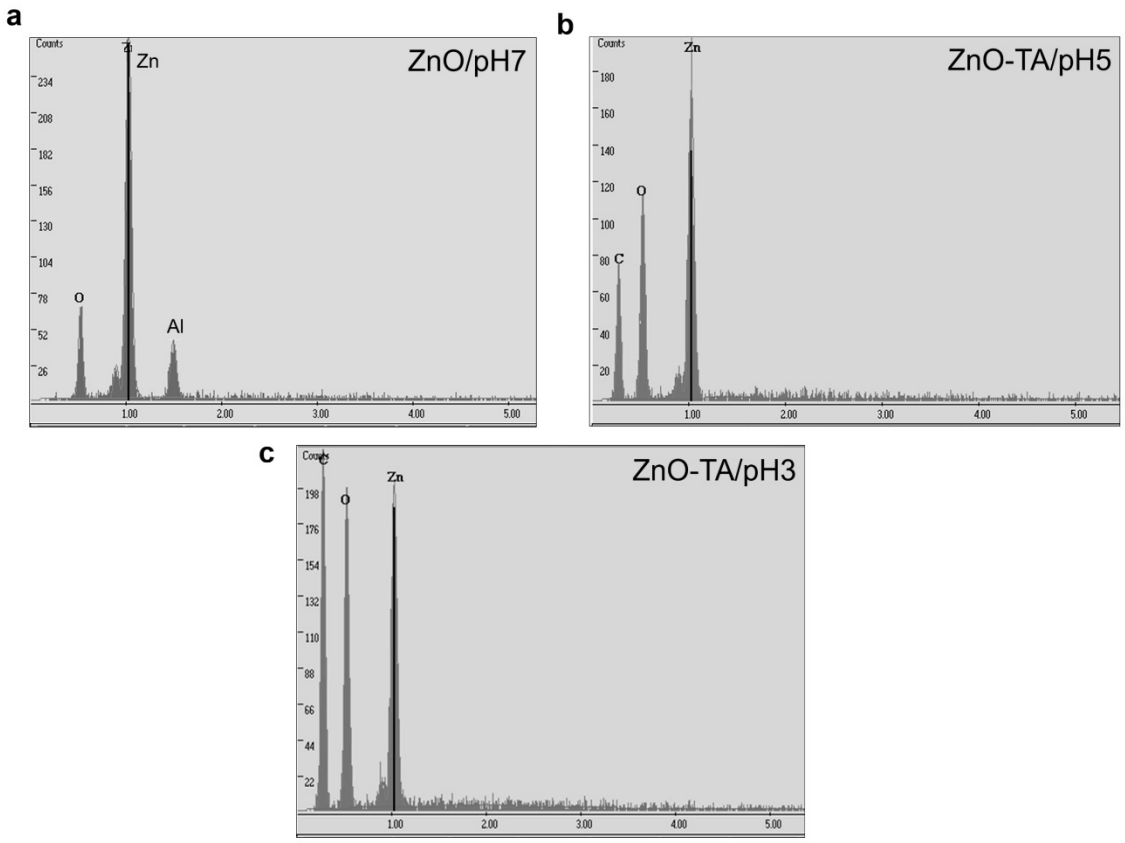

Figure 2: The corresponding surface elemental composition of pure ZnO and ZnO-TA nanostructures determined by EDX: (a) ZnO at pH 7, (b) ZnO–TA at pH 5, and (c) ZnO–TA at pH 3, indicating the relative weight percentages of Zn, O, C and Al, with the latter attributed to the use of Al foil as the substrate.

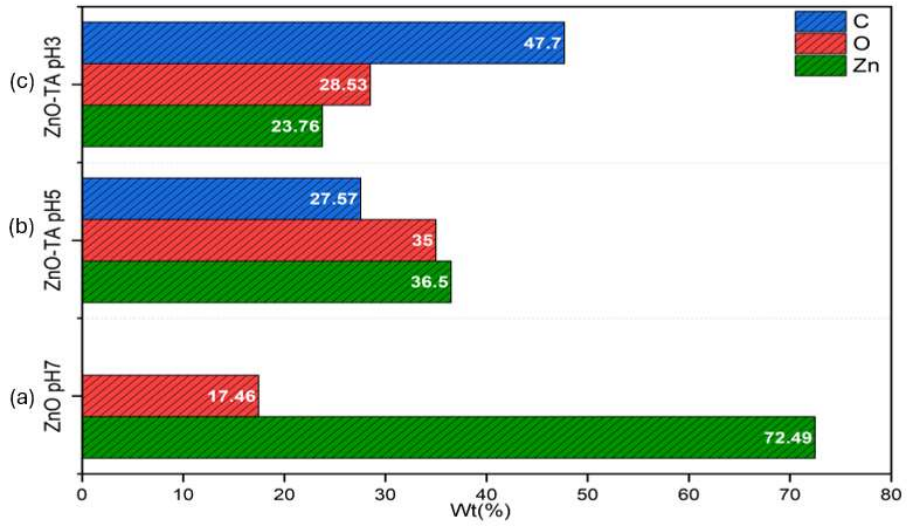

Figure 3: Elemental distribution maps of ZnO and ZnO–TA nanostructures synthesis at (a) pH7, (b) pH5 and (c) pH 3 obtained via FESEM–EDX analysis (from figures 1 and 2), illustrating the spatial dispersion of key elements and the effect of TA incorporation under varying synthesis conditions. The elemental maps indicate Zn in green, O in red, and C in blue.

The addition of TA induces a notable shift in the synthesis pH, transitioning from neutral (pH 7) to more acidic conditions (pH 5 and pH 3). TA functions as a stabilizing agent, leveraging its abundance of phenolic and carboxylic functional groups to influence the nucleation and growth dynamics of ZnO nanostructures. Upon TA incorporation, the sample synthesized at pH 5 retained the nanorod morphology observed at pH 7. However, the distribution was comparatively reduced, with some nanorods forming interconnected structures indicative of mild aggregation. This behaviour is likely attributable to TA-mediated surface interactions. Elemental analysis revealed a decrease in Zn content to 36.5%, accompanied by elevated concentrations of C (27.57%) and O (35%), suggesting moderate surface modification. These compositional changes may result from chelation or adsorption of TA's functional groups onto Zn^{2+} ions. In the absence of conventional surfactants, capillary forces become more pronounced; promoting agglomeration and interparticle adhesion, factors that may further influence the structural and electronic properties of the resulting nanomaterials [21, 22].

At pH 3, the influence of TA becomes markedly pronounced, resulting in the formation of highly interconnected nanostructural networks accompanied by evident aggregation and agglomeration. Elemental analysis reveals a substantial reduction in Zn content to 23.76%, while C reaches its highest concentration at 47.7%. Under these acidic conditions, TA exhibits enhanced solubility and reactivity, facilitating extensive surface capping and partial organic coating of the ZnO nanostructures. The increased acidity, driven by higher TA concentrations, promotes greater adsorption of TA onto the ZnO surface, leading to the formation of a thick organic layer. This layer not only contributes to elevated carbon incorporation but may also inhibit ZnO crystallization. Such extensive surface modification is particularly advantageous for applications requiring enhanced organic functionality, such as biosensing. The abundance of phenolic and carboxylate groups under low pH conditions contributes to significant carbon deposition, which in turn influences the morphological characteristics of the ZnO nanostructures. The incorporation of C species into the ZnO lattice may introduce structural defects, resulting in fragmentation or a reduction in nanorod dimensions. Furthermore, the presence of C-rich domains promotes surface irregularities, weakening the structural integrity of the nanorods and rendering them more susceptible to mechanical disruption [23–25].

The observed compositional trends align with the underlying principles of hydrothermal and green synthesis methodologies. Under neutral pH conditions, conventional hydrothermal synthesis favours the formation of pure, crystalline ZnO nanostructures with high Zn content. In contrast, the green hydrothermal approach employing TA at lower pH levels yields C-rich, surface-functionalized ZnO nanostructures. The tunability of this synthesis strategy enables controlled incorporation of organic moieties, offering a versatile route for engineering surface functionality and tailoring material properties for advanced applications.

3.2 Chemical Bonding Analysis of the Thin Film Samples

FTIR spectroscopy was employed to investigate the chemical bonding and surface modifications of pure ZnO and ZnO–TA nanostructures. This technique enables the identification of specific functional groups and provides comparative spectral insights into the role of phytochemicals and capping agents in stabilizing and modifying the nanomaterial surfaces, as illustrated in **Figure 4**. The FTIR spectra for all samples confirmed the presence of Zn–O stretching vibrations within the 600–900 cm^{-1} region, characteristic of ZnO lattice modes [26–29]. As the concentration of TA increased, corresponding to lower pH conditions, the fingerprint region of the spectra became increasingly dominated by features associated with TA. Notably, significant stretching vibrations were observed between 1000 and 1300 cm^{-1}. The pure ZnO sample exhibited distinct peaks at 1060 cm^{-1} and 1360 cm^{-1}, while the ZnO–TA samples displayed multiple additional peaks within this range. These features are attributed to carbonyl group (O–C–O) bonding.

Furthermore, all samples exhibited prominent absorption bands around 1600 cm^{-1}, corresponding to C=O and C–O stretching vibrations, indicative of carbonyl functionalities [30]. The presence of these bonding types resulted from atmospheric adsorption during the synthesis of the sample under non-vacuum conditions [31–33]. These bonding types are likely the result of atmospheric adsorption during synthesis under non-vacuum conditions [31–33]. The TA-modified samples (pH 5 and pH 3) also showed additional absorption bands between 1037 and 1208 cm^{-1}, associated with C–O–C stretching, and between 1349 and 1613 cm^{-1}, corresponding to C=O stretching—both characteristic of saturated ester groups [34,35]. Additionally, absorption bands within similar spectral regions were attributed to phenolic and carboxylate moieties present in TA. The intensities of O–H and –COOH-related peaks increased with decreasing pH, suggesting enhanced protonation and a greater presence of unbound TA molecules. This trend indicates stronger interactions between TA and the ZnO surface under acidic conditions, which further altering the surface chemistry of the nanostructures. A broad absorption band observed in the 3200–3300 cm^{-1} regions across all samples is attributed to hydroxyl stretching vibrations. This feature is likely associated with residual surface-bound hydroxyl groups formed during the dehydration process, which occurred consistently across all synthesis conditions [36, 37]. These parameters are indicative of the electronic structure and reactivity of the material and are particularly relevant in evaluating the influence of surface modifications and functional groups on the overall stability and performance of ZnO-based nanostructures [38, 39].

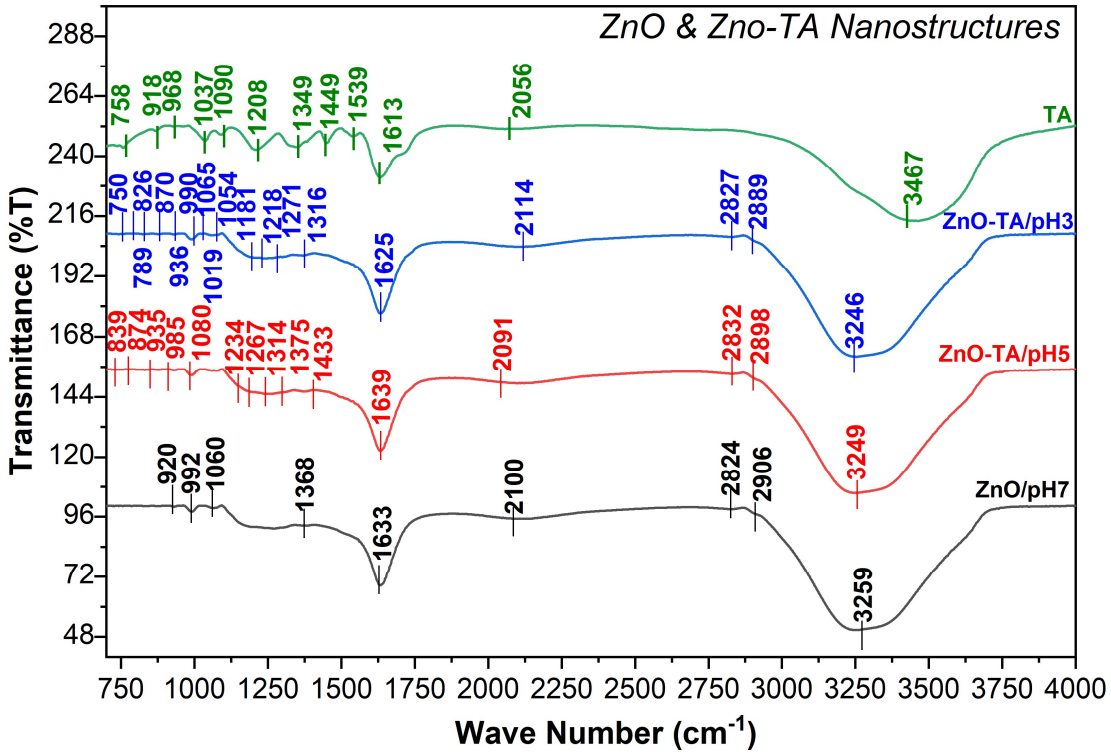

Figure 4: FTIR spectra of pure TA (green), ZnO–TA at pH 3 (blue), ZnO–TA at pH 5 (red), and pure ZnO at pH 7 (black), highlighting the characteristic vibrational stretching modes and the influence of TA incorporation under varying pH conditions on surface functional groups.

In addition, according to the Brønsted–Lowry acid–base theory, the formation of hydroxide ions (OH^-) arises from the interaction of ZnO with water, wherein ZnO can act as either a proton acceptor or donor depending on the surrounding chemical environment. In this context, ZnO behaves as a Brønsted–Lowry base by accepting protons, leading to the formation of zinc hydroxide ($Zn(OH)_2$). This reaction not only influences the surface chemistry but also alters the electronic structure of the material. The incorporation of hydroxide ions modifies the local electronic environment of the ZnO nanostructure, which can significantly impact its optical and electronic behaviour.

Such surface interactions are particularly pronounced at the interface regions, where Zn^{2+} ions (electron acceptors) and O^{2-} ions (electron donors) are in close proximity. These interfacial zones, characterized by variations in electron affinity and ionization potential, provide a favourable landscape for charge transfer processes. This facilitates exciton dissociation and contributes to morphological transformations of ZnO when exposed to specific substances, such as TAs, under controlled conditions. The dynamic nature of these interactions underscores the importance of surface chemistry in tuning the functional properties of ZnO-based nanostructures.

3.3 Electrical and Hall Coefficient of the ZnO and ZnO/PET Thin Film

The electrical characteristics of ZnO/PET and ZnO–TA/PET thin films were systematically investigated via *I–V* measurements employing a four-point probe configuration, as depicted in **Figure 5**. The observed linearity in the *I–V* profiles, in accordance with Ohm's law, is indicative of metallic-like conduction behaviour. This linear response confirms the establishment of a continuous and efficient charge transport pathway throughout the substrate matrix, which is essential for enhanced electrical conductivity.

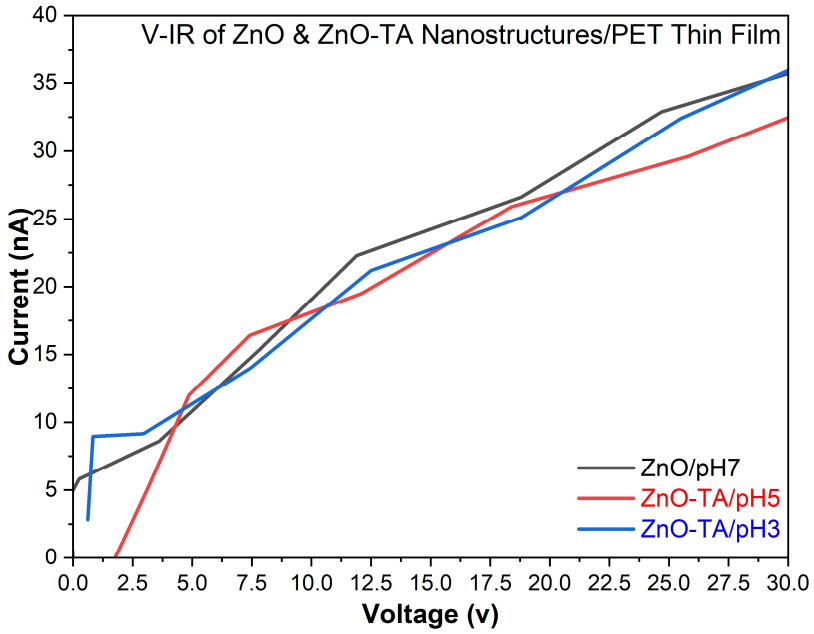

Figure 5: Current–Voltage (I–V) characteristics of ZnO and ZnO–TA nanostructures synthesized at varying pH levels, illustrating the influence of TA concentration on charge transport behaviour.

The lateral electrical conductivity, σ values derived from the *I–V* for ZnO and ZnO–TA thin films deposited on PET substrates, are summarized in **Table 1**. These measurements, obtained via a four-point probe technique, revealed conductivity values in the range of 10^{-8} S cm^{-1}, specifically ~16.45 ± 0.09 × 10^{-8} S cm^{-1} for ZnO/pH 7, ~7.736 ± 0.19 × 10^{-8} S cm^{-1} for ZnO-TA/pH 5, and ~10.66 ± 0.16 × 10^{-8} S cm^{-1} for ZnO-TA/pH 3. All three samples demonstrated markedly higher σ compared to previously reported pure ZnO nanostructured thin films, which typically exhibit σ values between ~5 × 10^{-10} and 3 × 10^{-8} S cm^{-1} [40]. This improvement underscores the effectiveness of the synthesis strategy in facilitating charge transport across the ZnO and ZnO–TA thin films deposited on PET substrates. It is noteworthy, however, that a slight reduction in σ was observed upon the incorporation of TA at pH 5. This attenuation is attributed to specific chemical interactions between TA and the ZnO surface. As previously discussed, TA contains multiple hydroxyl and carboxyl functional groups, with the carboxyl moieties capable of forming coordination

complexes with Zn^{2+} ions. These interactions may induce surface passivation or partially disrupt the continuity of conductive pathways, particularly at grain boundaries or surface regions where organic species are introduced. Such modifications can hinder electron mobility and contribute to the observed decline in conductivity [41]. These modifications can impede electron mobility and contribute to the observed decrease in σ.

Table 1: Summary of lateral **conductivityσ**, carrier **concentrationN_b**, electron mobility μ_h and the calculated of the average Hall Coefficient R_{sh} in ZnO and ZnO–TA/PET thin films.

Sample	σ ($\times 10^{-8}$ S.cm^{-1})	N_b ($\times 10^{15}$ cm^{-3})	μ_h (cm^2/V·s)	Avg. of Hall Coeff., R_H ($\times 10^3$ cm^3.C^{-1})
ZnO/pH7	16.45 ± 0.09	3.01 ± 1.13	1.64 ± 0.65	-0.23
ZnO-TA/pH5	7.736 ± 0.19	2.24 ± 1.09	2.59 ± 1.71	-2.69
ZnO-TA/pH3	10.66 ± 0.16	4.91 ± 2.14	1.16 ± 0.85	-1.62

A further reduction in σ was observed in the ZnO–TA/pH 3/PET thin film, following the addition of TA, when compared to the control ZnO/pH 7/PET thin film sample. However, this sample exhibited a modest increase in σ relative to the layer of thin film of ZnO–TA/pH 5/PET. This variation is closely linked to morphological changes, as evidenced by FESEM analysis. For ZnO-TA/pH5 on PET thin film, the ZnO nanostructures retained their nanorod morphology, although partial disaggregation of particles was apparent due to the presence of TA. In contrast, the sample prepared at pH 3 displayed a pronounced structural transformation, characterized by the near-complete absence of nanorods and the emergence of an amorphous, interconnected network of nanoparticles. This morphological shift is attributed to the increased concentration of TA, which introduces a higher density of carboxyl and hydroxyl functional groups, as confirmed by FTIR. These functional groups interact more extensively with the ZnO surface, and while they may initially act as insulating moieties, their elevated concentration can effectively passivate surface defects and reduce the density of electron trap states, thereby facilitating improved charge transport [42]. The compact and interconnected architecture observed in the ZnO–TA sample synthesized at pH 3 promotes enhanced structural coherence and facilitates efficient electron percolation pathways. This reduction in grain boundaries and structural discontinuities, features that typically hinder electron mobility, supports the observed improvement in σ of the thin film deposited on the PET substrate. These findings highlight the critical role of TA concentration in modulating both the morphology and electronic properties of ZnO-based nanostructures.

This behaviour is further illustrated in **Figure 6**, which schematically depicts the role of TA in influencing ZnO nanostructure formation and film performance. At pH 5, partial deprotonation imparts a

mild negative charge to TA molecules, which cap individual ZnO nanoparticles and disrupt interparticle connectivity, resulting in reduced conductivity. In contrast, at pH 3, TA is more fully protonated and acts as a structural linker, bridging ZnO nanoparticles to form a dense, interconnected network. This network enhances charge transport across the PET-supported thin film, demonstrating the potential of pH-controlled TA incorporation for optimizing ZnO-based materials in flexible electronic applications.

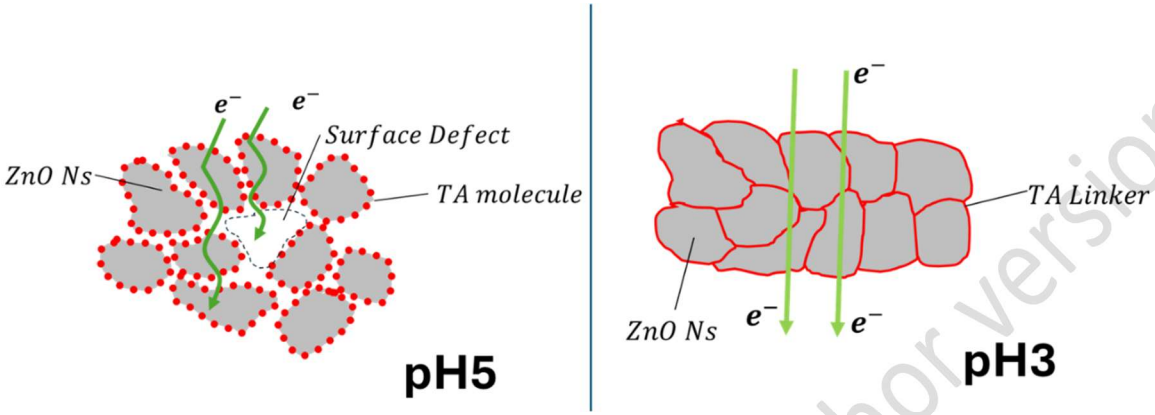

Figure 6: Schematic illustration of the role of tannic acid (TA) in modulating ZnO nanostructure connectivity. At pH 5, partially deprotonated TA caps individual nanoparticles, limiting interparticle linkage and reducing conductivity. At pH 3, fully protonated TA acts as a molecular bridge, promoting dense interconnectivity and enhancing conductivity in the ZnO–TA thin film on PET substrate.

To gain a more comprehensive understanding of the charge transport mechanisms within the fabricated thin films, Hall effect measurements were performed to determine the average Hall coefficientR_H, carrier concentrationN_b, and Hall mobility μ_h. All samples exhibited *n*-type conductivity, consistent with the intrinsic electronic behaviour of ZnO, which is known to possess native oxygen vacancies that act as donor states [40]. The carrier concentration was found to be on the order of 10^{15} cm^{-3}, aligning well with previously reported values for undoped ZnO thin film [43-45]. Among the samples analyzed, the ZnO–TA/pH5/PET thin film demonstrated the highest μ_h, suggesting improved charge transport efficiency. In contrast, the ZnO–TA/pH5/PET thin film exhibited a reduction in μ_h, which is likely attributable to increased grain boundary scattering resulting from particle aggregation. These findings highlight the sensitivity of charge transport properties to both surface chemistry and morphological features, which are modulated by the concentration of TA and the synthesis conditions.

The R_H exhibited an inverse relationship with carrier concentration, whereby thin film samples with higher carrier densities displayed correspondingly lower R_H values. This trend reflects the increased availability of free charge carriers within the transport medium [46], a phenomenon well-documented in semiconductor systems, including ZnO nanostructures [47]. A comprehensive summary of the Hall measurements for all thin film samples is presented in **Table 1**. For the ZnO/pH 7/PET thin film, the N_b was

measured at 3.01 ± 1.13 × 10^{15} cm^{-3}, accompanied by μ_h of 1.64 ± 0.65 $cm^2\ V^{-1}\ s^{-1}$ and a R_H of –0.23 × 10^3 $cm^3\ C^{-1}$. These values are characteristic of intrinsic ZnO, where *n*-type conductivity arises primarily from native oxygen vacancies. The moderate mobility observed is likely constrained by the presence of surface trap states and grain boundary scattering, which limit the efficiency of charge transport across the film.

For the ZnO–TA/pH5/PET thin film, the thin film exhibited enhanced μ_h (2.59 ± 1.71 $cm^2\ V^{-1}\ s^{-1}$), despite a slight reduction in N_b(2.24 ± 1.09 × 10^{15} cm^{-3}), and a corresponding R_H of –1.62 × 10^3 $cm^3\ C^{-1}$. This improvement is attributed to the passivation of surface trap states by phenolic hydroxyl groups in TA, which reduce electron scattering and facilitate smoother charge transport pathways [49–51]. For ZnO-TA/pH 3/PET thin film, N_b , has been increased to 4.91 ± 2.14 × 10^{15} cm^{-3}. However, this was accompanied by a notable decline in μ_h (1.16 ± 0.85 $cm^2\ V^{-1}\ s^{-1}$) and a R_H of –2.69 × 10^3 $cm^3\ C^{-1}$. The reduced μ_h is ascribed to excessive particle aggregation and elevated grain boundary density, which act as scattering centres and hinder charge transport. Another plausible explanation for the observed decrease in conductivity at pH 5, despite an increase in μ_h, lies in the reduction of N_b due to chemical interactions between TA and ZnO. At pH 5, the partial complexation of Zn^{2+} ions by TA's carboxyl groups may interfere with the formation of native oxygen vacancies, which are the primary source of free electrons in intrinsic ZnO. This reduction in donor defects leads to a lower carrier concentration, thereby decreasing the overall σ as σ is directly proportional to both mobility μ_h and N_b given by $\sigma = n\mu e$. While the μ_h increases due to improved local ordering or reduced phonon scattering within grains, the diminished carrier density limits the total number of charge carriers available for conduction, resulting in a net decrease in σ . This highlights the delicate balance between chemical surface modification and intrinsic defect chemistry in determining the electronic performance of ZnO–TA thin films. These findings underscore the critical role of surface chemistry and TA concentration in modulating the structural and electronic properties of nano ZnO-based thin film.

In this case, the multiple hydroxyl and phenolic functional groups of TA can interact with surface defects and dangling bonds on ZnO nanostructures. These interactions contribute to trap passivation by neutralizing surface states that would otherwise act as recombination centers or scattering sites for charge carriers. By reducing the density of surface trap states, TA functionalization helps suppress carrier trapping and enhances the continuity of charged transport pathways. Additionally, the chelating nature of TA can promote better particle dispersion and interfacial bonding, leading to improved film uniformity and reduced grain boundary resistance. These effects collectively contribute to a modest enhancement in carrier mobility and electrical conductivity, particularly in the ZnO–TA/pH 3/PET sample, where the interconnected nanoparticle network benefits from both structural and chemical stabilization provided by TA. Optimal TA incorporation enhances σ and μ_h, whereas excessive amounts induce structural disorder that compromises electronic performance.

Herein, both ZnO/pH 7/PET and ZnO–TA/pH 3/PET thin films exhibit distinct structural and electronic characteristics that offer specific advantages depending on the target application. The ZnO/pH 7/PET thin film displays a well-defined nanorod morphology, indicative of high crystallinity and superior intrinsic σ. This anisotropic structure supports directional charge transport with minimal scattering, making it particularly suitable for high-performance optoelectronic devices where mobility and structural order are critical. In contrast, the ZnO–TA/pH 3/PET thin film features an amorphous, interconnected nanoparticle network resulting from the disruption of nanorods due to elevated TA concentration. Although this morphology leads to reduced electron mobility, primarily due to grain boundary scattering, it facilitates enhanced percolation pathways and yields a modest improvement in σ compared to the ZnO–TA/pH 5/PET sample. This configuration is advantageous for flexible and wearable electronics, where uniform film coverage, mechanical compliance, and stable conductivity are prioritised over high mobility. Therefore, while ZnO/pH 7/PET may be optimal for applications requiring high-speed charge transport and structural precision, ZnO–TA/pH 3/PET offers practical benefits in emerging technologies that demand flexibility and robust electrical performance. The selection of the optimal system should be guided by the specific functional requirements of the intended application.

4. Conclusion

A comprehensive evaluation of ZnO and ZnO–TA nanostructures, synthesized via hydrothermal methods and subsequently deposited as thin films onto PET substrates, reveals the significant influence of TA on their morphological, chemical and electrical properties. Morphological analysis conducted on the precursor solutions prior to deposition, using FESEM, showed a transition from well-defined ZnO nanorods at pH 7 to increasingly aggregated and amorphous nanoparticle networks at lower pH levels, particularly pH 3. This transformation is attributed to strong interactions between TA's functional groups and ZnO particles, which disrupt the original nanorod architecture.

FTIR performed on the deposited thin films confirmed the presence of organic functionalities introduced by TA, notably hydroxyl and carboxyl groups, which modified the surface chemistry of the ZnO–TA films. Electrical characterisation, conducted on the thin films deposited on PET substrates, demonstrated that the pristine ZnO sample (pH 7) exhibited the highest σ. However, the ZnO–TA/pH5/PET thin film showed enhanced μ_h, attributed to the passivation of surface trap states by TA, which facilitated more efficient charge transport despite a slight reduction in carrier concentration.

In contrast, the ZnO–TA/pH3/PET thin film exhibited an increase in N_b but a noticeable reduction in μ_h. This decline is attributed to particle aggregation and elevated grain boundary density, which act as scattering centres and hinder charge transport. Despite these limitations, the thin film demonstrated a modest

enhancement in σ compared to the ZnO–TA/pH5/PET thin film, suggesting that the interconnected nanoparticle network formed at lower pH levels may facilitate improved percolation pathways. These electrical measurements, conducted directly on the PET-supported thin films, highlight the critical role of substrate–film interactions and surface morphology in determining charge transport behaviour. The findings reinforce the importance of optimizing TA concentration to achieve balanced structural and electronic performance in ZnO-based thin films for flexible electronic applications.

Acknowledgement

University Malaysia Pahang Al-Sultan Abdullah (UMPSA) fully supports the facilities and resources for this research. The authors would like to acknowledge the support of the internal grants of University Malaysia Pahang Al-Sultan Abdullah (RDU2203105).

Declarations

Ethical Approval

The authors declare no conflict of interest.

Competing interests

The authors declare no competing interests.

Authors Contribution

Conceptualization, N.A.C.L.; methodology, N.A.C.L.; software, N.A.C.L.; validation, N.A.C.L. and A.K.; formal analysis, N.A.C.L. and A.K.; investigation, A.K.; resources, N.A.C.L.; data curation, A.K.; writing—original draft preparation, A.K.; writing—review and editing, A.K.; visualization, A.K.; supervision, N.A.C.L.; project administration, N.A.C.L.; funding acquisition, N.A.C.L. All authors have read and agreed to the published version of the manuscript.

Funding

The research work is entirely funded by the internal grants of Universiti Malaysia Pahang Al- Sultan Abdullah (RDU2203105).

Availability of data and materials

The raw/processed data required to reproduce these findings cannot be shared as the data also forms part of an ongoing study. Further information on the data is available from the corresponding authors upon reasonable request.

References

1. Bouacheria MA, Djelloul A, Adnane M, Larbah Y, Benharrat L. Characterization of Pure and Al Doped ZnO Thin Films Prepared by Sol Gel Method for Solar Cell Applications. J Inorg Organomet Polym Mater [Internet] 2022;32:2737–47. Available from: https://doi.org/10.1007/s10904-022-02313-0

2. Sreedev P, Rakhesh V, Roshima NS. Optical characterization of ZnO thin films prepared by Chemical bath deposition method. IOP Conf Ser Mater Sci Eng [Internet] 2018;377:012086. Available from: https://dx.doi.org/10.1088/1757-899X/377/1/012086

3. Saeed M, Marwani HM, Shahzad U, Asiri AM, Rahman MM. Recent Advances, Challenges, and Future Perspectives of ZnO Nanostructure Materials Towards Energy Applications. The Chemical Record [Internet] 2024;24:e202300106. Available from: https://doi.org/10.1002/tcr.202300106

4. Selvarajan E, Mohanasrinivasan V. Biosynthesis and characterization of ZnO nanoparticles using Lactobacillus plantarum VITES07. Mater Lett 2013;112:180–2.

5. Akinlotan OO, Ezenobi U v. A REVIEW OF VARIOUS METHODS OF SYNTHESIZING NANOPARTICLES AND THEIR APPLICATIONS . Journal of Chemical Society of Nigeria [Internet] 2020;45. Available from: https://www.journals.chemsociety.org.ng/index.php/jcsn/article/view/489

6. Ahmad T. Reviewing the Tannic Acid Mediated Synthesis of Metal Nanoparticles. 2014;2014.

7. Rahal B, Boudine B, Larbah Y, Siad M, Souami N. Influence of Low Cd-Doping Concentration (0.5 and 3 wt.%) and Different Substrate Types (Glass and Silicon) on the Properties of Dip-Coated Nanostructured ZnO Semiconductors Thin Films. J Inorg Organomet Polym Mater [Internet] 2021;31:4001–17. Available from: https://doi.org/10.1007/s10904-021-02024-y

8. More P, Inamdar V, Suresh S, Dindorkar S, Peddakolmi S, Jain K, et al. Synthesis of zinc oxide nanoparticles using Chrysopogonzizanioides grass extract, its applications in photodegradation and antimicrobial activity. Journal of Materials Science: Materials in Electronics [Internet] 2021;32:20725–41. Available from: https://doi.org/10.1007/s10854-021-06585-z

9. Ansari Z, Kadam S, Salve V, Patil K, Wadhawa G, More P. Structural, electrochemical, and photoelectrochemical performance of Cr doped ZnO@rGO nanocomposites synthesized via Sol-Gel and hydrothermal methods. J Mol Struct [Internet] 2026;1349:143761. Available from: https://www.sciencedirect.com/science/article/pii/S0022286025024202

10. Lou W, Chen Y, Ma H, Liang G, Liu B. Antioxidant and α-amylase inhibitory activities of tannic acid. J Food Sci Technol [Internet] 2018;55:3640–6. Available from: https://doi.org/10.1007/s13197-018-3292-x

11. Hazer B, Ashby RD. Synthesis of a novel tannic acid-functionalized polypropylene as antioxidant active-packaging materials. Food Chem [Internet] 2021;344:128644. Available from: https://www.sciencedirect.com/science/article/pii/S0308814620325061

12. Guo J, Sun W, Kim JP, Lu X, Li Q, Lin M, et al. Development of tannin-inspired antimicrobial bioadhesives. Acta Biomater [Internet] 2018;72:35–44. Available from: https://www.sciencedirect.com/science/article/pii/S1742706118301284

13. Baer-Dubowska W, Szaefer H, Majchrzak-Celińska A, Krajka-Kuźniak V. Tannic Acid: Specific Form of Tannins in Cancer Chemoprevention and Therapy-Old and New Applications. Curr Pharmacol Rep [Internet] 2020;6:28–37. Available from: https://doi.org/10.1007/s40495-020-00211-y

14. Kaczmarek B. Tannic Acid with Antiviral and Antibacterial Activity as A Promising Component of Biomaterials—A Minireview. Materials [Internet] 2020;13. Available from: https://www.mdpi.com/1996-1944/13/14/3224

15. Nagarajan S, Arumugam Kuppusamy K. Extracellular synthesis of zinc oxide nanoparticle using seaweeds of gulf of Mannar, India. J Nanobiotechnology [Internet] 2013;11:39. Available from: https://doi.org/10.1186/1477-3155-11-39

16. Yu S, Zhang H, Zhang J, Li Z. Effects of pH on High-Performance ZnO Resistive Humidity Sensors Using One-Step Synthesis. Sensors [Internet] 2019;19. Available from: https://www.mdpi.com/1424-8220/19/23/5267

17. Agale P, Salve V, Arade S, Balgude S, More P. Tailoring structural and chemical properties of ZnO@ g-C3N4 nanocomposites through Sr doping: Insights from multi technique characterization. Solid State Sci [Internet] 2025;166:107960. Available from: https://www.sciencedirect.com/science/article/pii/S1293255825001384

18. Ansari Z, Kadam S, Kasabe S, Tripathi J, Agale P, Patange S, More P. Optimized Mn doped ZnO@rGO nanocomposites: a breakthrough for advanced energy storage and PEC systems. Ionics [Internet]. 2025;31:8151–8172. Available from: https://doi.org/10.1007/s11581-025-06468-x

19. Larbah Y, Adnane M, Rahal B. Growth and Characterization of ZnO and Al-Doped ZnO Thin Films by a Homemade Spray Pyrolysis. Semiconductors [Internet] 2020;54:1439–44. Available from: https://doi.org/10.1134/S1063782620110184

20. Sadeghi B. Controlled Growth and Characterization Ag/ZnO Nanotetrapods for Humidity Sensing. Comb Chem High Throughput Screen 2018;21.

21. Donia DT, Bauer EM, Missori M, Roselli L, Cecchetti D, Tagliatesta P, et al. Room Temperature Syntheses of ZnO and Their Structures. Symmetry (Basel) [Internet] 2021;13. Available from: https://www.mdpi.com/2073-8994/13/4/733

22. Abdelmohsen AH, Rouby WMA El, Ismail N, Farghali AA. Morphology Transition Engineering of ZnO Nanorods to Nanoplatelets Grafted Mo8O23-MoO2 by Polyoxometalates: Mechanism and Possible Applicability to other Oxides. Sci Rep [Internet] 2017;7:5946. Available from: https://doi.org/10.1038/s41598-017-05750-x

23. Honda M, Tokuda F, Ichikawa Y. Effects of carbon defects on ZnO nanorods directly grown on graphene. Jpn J Appl Phys [Internet] 2017;56:110306. Available from: https://dx.doi.org/10.7567/JJAP.56.110306

24. Louis J, Padmanabhan NT, Jayaraj MK, John H. Crystal lattice engineering in a screw-dislocated ZnO nanocone photocatalyst by carbon doping. Mater Adv [Internet] 2022;3:4322–33. Available from: http://dx.doi.org/10.1039/D2MA00098A

25. Sahu J, Kumar S, Vats VS, Alvi PA, Dalela B, Phase DM, et al. Role of defects and oxygen vacancy on structural, optical and electronic structure properties in Sm-substituted ZnO nanomaterials. Journal of Materials Science: Materials in Electronics [Internet] 2022;33:21546–68. Available from: https://doi.org/10.1007/s10854-022-08945-9

26. Balogun SW, James OO, Sanusi YK, Olayinka OH. Green synthesis and characterization of zinc oxide nanoparticles using bashful (Mimosa pudica), leaf extract: a precursor for organic electronics applications. SN Appl Sci [Internet] 2020;2:504. Available from: https://doi.org/10.1007/s42452-020-2127-3

27. Amutha C, Thanikaikarasan S, Ramadas V, Bahadur SA, Natarajan B, Kalyani R. Synthesis, characterization and antibacterial efficiency of ZnO nanoparticles using rice as soft bio-template. Optik (Stuttg) [Internet] 2016;127:4281–6. Available from: https://www.sciencedirect.com/science/article/pii/S003040261600173X

28. Kumar A, Khatana C, Kumar D, Kumari A. Antibacterial Potential of Zinc Oxide Nanoparticles Synthesized using Aloe vera (L.) Burm.f.: A Green Approach to Combat Drug Resistance. J Pure Appl Microbiol 2021;15.

29. Krysova H, Mansfeldova V, Tarabkova H, Pisarikova A, Hubicka Z, Kavan L. High-quality dense ZnO thin films: work function and photo/electrochemical properties. Journal of Solid State Electrochemistry [Internet] 2024;28:2531–46. Available from: https://doi.org/10.1007/s10008-023-05766-6

30. Meng FB, Li JJ, Zhang Q, Li YC, Liu DY, Chen WJ, et al. Complex wall materials of polysaccharide and protein effectively protected numb-taste substance degradation of Zanthoxylum bungeanum. J Sci Food Agric [Internet] 2021;101:4605–12. Available from: https://doi.org/10.1002/jsfa.11103

31. Sahu M, Reddy VRM, Kim B, Patro B, Park C, Kim WK, et al. Fabrication of Cu2ZnSnS4 Light Absorber Using a Cost-Effective Mechanochemical Method for Photovoltaic Applications. Materials [Internet] 2022;15. Available from: https://www.mdpi.com/1996-1944/15/5/1708

32. Dillip GR, Banerjee AN, Anitha VC, Joo SW, Min BK, Sawant SY, et al. Anchoring Mechanism of ZnO Nanoparticles on Graphitic Carbon Nanofiber Surfaces through a Modified Co-Precipitation Method to Improve Interfacial Contact and Photocatalytic Performance. ChemPhysChem [Internet] 2015;16:3214–32. Available from: https://doi.org/10.1002/cphc.201500529

33. Enumo A, Gross IP, Saatkamp RH, Pires ATN, Parize AL. Evaluation of mechanical, thermal and morphological properties of PLA films plasticized with maleic acid and its propyl ester derivatives. Polym Test [Internet] 2020;88:106552. Available from: https://www.sciencedirect.com/science/article/pii/S0142941820303263

34. Boughrara L, Zaoui F, Guezzoul M, Sebba FZ, Bounaceur B, Kada SO. New alginic acid derivatives ester for methylene blue dye adsorption: kinetic, isotherm, thermodynamic, and mechanism study. Int J Biol Macromol [Internet] 2022;205:651–63. Available from: https://www.sciencedirect.com/science/article/pii/S0141813022003348

35. Krithika R, Balasasirekha R. FTIR SPECTRUM AND XRD OF POSTBIOTICS-EXOPOLYSACCHARIDES ZINC OXIDE NANOPARTICLES [Internet]. 2021. Available from: http://www.sciensage.info

36. Mecozzi M, Sturchio E. Computer Assisted Examination of Infrared and Near Infrared Spectra to Assess Structural and Molecular Changes in Biological Samples Exposed to Pollutants: A Case of Study. J Imaging 2017;3.

37. Kateris N, Jayaraman AS, Wang H. HOMO-LUMO gaps of large polycyclic aromatic hydrocarbons and their implication on the quantum confinement behavior of flame-formed carbon nanoparticles. Proceedings of the Combustion Institute [Internet] 2023;39:1069–77. Available from: https://www.sciencedirect.com/science/article/pii/S1540748922001900

38. Dejpasand MT, Saievar-Iranizad E, Bayat A, Montaghemi A, Ardekani SR. Tuning HOMO and LUMO of three region (UV, Vis and IR) photoluminescent nitrogen doped graphene quantum dots for photodegradation of methylene blue. Mater Res Bull [Internet] 2020;128:110886. Available from: https://www.sciencedirect.com/science/article/pii/S002554082030413X

39. Panžić I, Capan I, Brodar T, Bafti A, Mandić V. Structural and Electrical Characterization of Pure and Al-Doped ZnO Nanorods. Materials [Internet] 2021;14. Available from: https://www.mdpi.com/1996-1944/14/23/7454

40. Che Lah NA, Kamaruzaman A. The physico-chemical and antimicrobial properties of nano ZnO functionalised tannic acid. Sci Rep [Internet] 2024;14:18596. Available from: https://doi.org/10.1038/s41598-024-69632-9

41. Radiev Y, Wollandt T, Klauk H, Witte G. Unveiling the Effects of Hydroxyl-Induced Trap States on the Charge Transport in p- and n-Channel Organic Field-Effect Transistors through Variable-Temperature Characterization. Advanced Materials [Internet] 2025;n/a:2505631. Available from: https://doi.org/10.1002/adma.202505631

42. Hanna B, Manuraj M, Surendran KP, Unni KNN. Opto-electronic properties of solution-processed zinc oxide thin films: role of solvents and doping. Journal of Materials Science: Materials in Electronics [Internet] 2020;31:13570–7. Available from: https://doi.org/10.1007/s10854-020-03913-7

43. Park JI, Lee HU, Pearson C, Petty MC, Jeong Y. Effects of Hydrogen Plasma Treatment on the Electrical Behavior of Solution-Processed ZnO Thin Films. Materials [Internet] 2024;17. Available from: https://www.mdpi.com/1996-1944/17/11/2673

44. Bakshi S, Rani S. Investigating the Impact of Annealing and Thickness on the Optical and Electrical Characteristics of ZnO (TCO) for Optoelectronics Devices. Int. J. Thin. Fil. Sci. Tec 2025;14:139–49.

45. Al-Muntaser AA, Alzahrani E, Asnag GM, Yassin AY. Tailoring Structural, Optical, and Dielectric Properties of PVC/PMMA/PS/ZnO Nanocomposites for Capacitive Energy Storage Applications. ECS Journal of Solid State Science and Technology [Internet] 2025;14:033001. Available from: https://dx.doi.org/10.1149/2162-8777/adb992

46. Khan A ur R, Ramzan M, Imran M, Zubair M, Shahab S, Ahmed SJ, et al. Tailoring the Structural, Optical and Electrical Properties of Zinc Oxide Nanostructures by Zirconium Doping. Coatings [Internet] 2023;13. Available from: https://www.mdpi.com/2079-6412/13/1/34

47. Ghosh S, Basak D. Correlation between Hall Mobility and Optical Mobility in Aluminum-Doped ZnO Films via Boundary Scatterings and Estimation of Donor Compensation Ratio. physica status solidi (b) [Internet] 2020;257:1900682. Available from: https://onlinelibrary.wiley.com/doi/abs/10.1002/pssb.201900682